ELSEVIER

The linear growth of Görtler vortices

M. V. Finnis and A. Brown
School of Engineering and Applied Science, Royal Military College of Science,
Cranfield University, Shrivenham,
Swindon, UK

Measurements are presented of the streamwise velocity variation within a laminar boundary layer on a concave surface of 4-m radius of curvature for free-stream velocities of 7.5 and 10 m/s. The measured variation was consistent with the presence of counter-rotating vortices resulting from the Görtler instability. Contour plots of velocity and turbulence intensity show that the vortices occur in discrete pairs centred about upwash locations, rather than in a continuous row of counter-rotating vortices modelled by the stability analysis. Comparison with the normal-mode linear stability analysis indicates that the experimental data lie in a region of the stability chart for which the two observed conditions of streamwise development at constant wavelength and constant growth rate coincide. Disturbance velocity profiles compare favourably at streamwise positions for which the linear stability analysis is appropriate. Detailed comparison with the linear stability analysis indicates that the measured growth rates are considerably lower than those obtained from theory. (This is attributed to the limitations of the normal-mode analysis as well as to the fact that the observed vortices occur in discrete pairs often separated by regions of relatively undisturbed flow.) Although measured growth rates obtained by considering individual vortices were found to be greater than those obtained using spanwise-averaged velocity profiles.

Introduction

Görtler instability occurs as a consequence of the imbalance of centrifugal and pressure forces within the laminar boundary layer on a concave surface. The instability results in counter-rotating vortex pairs with their axes aligned in the flow direction. In a growing boundary layer, the vortices develop in the streamwise direction, increasing in amplitude, although maintaining a constant wavelength, until the flow breaks down to turbulence. The route to turbulence may be through the interaction with other boundary-layer disturbances, such as the Tollmien–Schlichting instability, or through the breakdown of secondary instabilities initiated at highly distorted regions of the boundary-layer flow.

It is generally recognised that the development of the Görtler instability is influenced by initial disturbances and that the leading-edge receptivity plays an important part in the resulting flow structure. Saric (1994) suggests that the theory is currently in advance of available experimental data and that detailed experiments in the linear growth regime are required with well-controlled leading-edge and free-stream conditions. The present work does not entirely fulfill this need, although it is hoped that future development will allow more extensive and detailed measurements to be made.

Görtler (1940) was the first to develop a linear stability analysis of a boundary-layer flow on a concave surface. He identified the parameter $Re_\theta(\theta/r)^{1/2}$, now commonly known as the Görtler number, as significant in indicating the stability of the boundary-layer flow. Liepmann (1945), extending earlier work in which he investigated the effects of curvature and pressure gradient on boundary-layer transition, correlated the Görtler number at transition with free-stream turbulence intensity. The results of Liepmann are often quoted and have been used as a basis of predicting transition on curved surfaces in general (e.g., Forest 1977).

The linear analysis of the Görtler instability is well established with the flow field being described by a mean flow with superimposed three-dimensional (3-D) disturbances in the form of counter-rotating vortices. Görtler (1940) assumed a parallel mean flow (in which the velocity terms normal to the surface were assumed to be zero) and disturbances that developed in time. The resulting analysis led to a three-parameter eigenvalue problem in the Görtler number G, the wave number ω, and a growth parameter $\beta\theta\,Re_\theta$ providing a universal stability chart. Görtler was primarily concerned with predicting the onset of the instability, although he recognised that the formation of the vortices would not necessarily indicate incipient turbulence of the flow.

Much of the theoretical work since that of Görtler (1940) has been concerned with refining the analysis, both in the formulation of and in the method of solving the governing equations. Smith (1955), in a quasiparallel analysis, retained the mean-flow normal velocity terms and made the intuitively more realistic assumption of the vortices growing with streamwise position rather than in time. However, he made the assumption that the streamwise variation of the disturbance profiles is small and, consequently, retained a growth factor. Smith simplified the resulting equations by ignoring terms that were considered to affect his coefficients by less than 1%. More recently, Floryan and Saric (1982), among others, have produced a correct order-of-magnitude formulation of the governing equations.

Address reprint requests to Prof. Alex Brown, School of Engineering and Applied Science, Royal Military College of Science, Cranfield University, Shrivenham, Swindon, SN6 8LA, UK.

Received 19 January 1996; accepted 20 November 1996

Int. J. Heat and Fluid Flow 18:389–399, 1997

655 Avenue of the Americas, New York, NY 10010

0142-727X/97/$17.00
PII S0142-727X(97)00022-2

The shape of the stability chart is influenced by the nature of the mean flow. For a surface with constant curvature, the stability chart is invariant for boundary layers with self-similar profiles, and, in general, the Görtler number increases with streamwise position. For boundary-layer flows that do not exhibit self-similarity, the stability chart will change with the shape of the mean-flow velocity profiles, and the Görtler number will not necessarily be a unique function of streamwise position.

Smith (1955), whilst agreeing that the Görtler number characterises the stability of flows on surfaces of constant curvature, postulated that ultimately the vortex amplitude determines the transition point. He correlated the then available experimental data with values of $\int \beta \, dx$, and concluded that transition was determined by $\int \beta \, dx \approx 10$.

The method of reducing the governing equations to a set of ordinary differential equations by assuming a constant growth rate to remove the streamwise dependence has come to be known as the local or normal-mode analysis. It is the classical approach to solving the Görtler problem and the results in an eigenvalue problem with the disturbance velocities appearing as the eigenfunction. For a review of the many variations of the normal-mode analysis the reader is referred to Herbert (1976).

Hall (1982) had questioned the validity of the quasiparallel assumption, and in Hall (1983), he solved a nonparallel formulation of the Görtler problem. Solution of the resulting partial differential equations was by a marching technique in which the development of an initial disturbance was followed downstream. Characterising the vortex growth by the disturbance energy, he found that the stability depended on the location and form of the initial disturbance. As a consequence, Hall concluded that it is not possible to determine a unique neutral stability curve for the Görtler problem.

More recently Hall (1990) investigated the leading-edge receptivity problem. Using a model of a free-stream longitudinal vortex impinging on the leading edge of a curved surface to provide initial conditions, a unique neutral stability curve was obtained, although it was found to be weakly dependent on the surface curvature.

Kalburgi et al. (1988a) and Day et al. (1990) have made detailed comparisons between the normal-mode analysis and the marching technique. Kalburgi et al. (1988b) have also compared solutions obtained using the marching technique with experimental measurements of the instability on an aerofoil.

A minor difficulty encountered in using the marching technique is how to define the growth rate. As described in Day et al. (1990), the particular definition chosen can affect the position of the neutral stability and which of two disturbances is more stable. Hall (1983) used an energy integral to monitor the development of a vortex; however, when making direct comparisons with the normal-mode analysis, or indeed with experimental measurements, it is appropriate to use the amplitude of the streamwise component of the disturbance in the manner of Kalburgi et al. (1988a, 1988b).

Kalburgi et al. (1988a, 1988b) attribute the various neutral curves of Hall (1983) to the use of unrealistic initial disturbances rather than to any fundamental fluid dynamic phenomenon. Furthermore, they concluded that for a Blasius mean flow and constant surface curvature, the normal-mode solutions are the "natural" solutions to the marching scheme and also its "natural" initial conditions. This was because whatever disturbance was selected as the initial condition, subsequent development was such that the disturbance approached the normal-mode solution. Also, if a normal-mode solution was used as a starting condition, then the marching scheme and normal-mode analysis gave identical downstream development. However, it was noted that on a surface with variable curvature, the disturbance velocity components were found to develop at different rates. For this situation, the normal-mode analysis will produce a different streamwise development to that of the marching scheme because of the restrictive assumption of uniform disturbance velocity growth rates.

Day et al. (1990) found modest differences between the normal-mode analysis and the marching scheme for the cases they investigated. They concluded that the normal-mode analysis might be used for engineering studies, perhaps with an empirical correction. They attributed the differences to the cumulative effect of marching in the streamwise direction. The history of the vortex development causes the marched disturbances to lag behind the "ideal" of the normal-mode analysis, which changes rapidly enough so that it is never reached. This results in lower growth rates being calculated using the marching scheme, as compared with those obtained from the normal-mode analysis.

Much of the effort in recent years has been in solving the nonlinear Görtler problem and the subsequent development of secondary instabilities. Recent numerical models of large amplitude Görtler instabilities have relied on solving the temporal development for a parallel flow formulation of the equations (Sabry and Liu, 1991; Liu and Domaradzki, 1993). This formulation has been criticised in Hall (1990), and more recently, Lee and Liu (1992) have investigated the problem of nonlinear spatially developing Görtler vortices. Initial conditions for many of the nonlinear solutions are generated using the quasiparallel linear analysis to provide the form of the disturbances and experimental data, often that of Swearingen and Blackwelder (1987), to provide the amplitude.

Early experimental work was confined to confirming the existence of Görtler vortices in a laminar boundary layer on a concave surface. Although visualisation of vortices had been mentioned in passing by Gregory and Walker (1956), the first measurements of the spanwise velocity variation within the

Notation

G	Görtler number, $\mathrm{Re}_\theta(\theta/r)^{1/2}$ (—)
Re_θ	Reynolds number based on θ, $(U_0\theta/\nu)$ (—)
Re_x	Reynolds number based on x, $(U_0 x/\nu)$ (—)
u, v, w	velocity components in the x, y, z directions, (m/s)
u_{av}	spanwise averaged streamwise velocity, (m/s)
u'	unsteady component of streamwise velocity, (m/s)
u_0	mean flow velocity component in the x-direction, (m/s)
u_1, v_1, w_1	disturbance velocity functions, (m/s)
U_0	measured free-stream velocity, (m/s)
x, y, z	streamwise, normal, and spanwise coordinates, m

Greek

α	wavenumber, $2\pi/\lambda$, m^{-1}
β	vortex growth rate, m^{-1}
δ	boundary-layer reference length, $x/\mathrm{Re}_x^{1/2}$, m
δ_L	boundary-layer thickness (99%) obtained from the Blasius solution, $4.91x/\mathrm{Re}_x^{1/2}$, m
θ	boundary-layer momentum thickness, m
κ_u	maximum value of streamwise disturbance velocity profile normalised with free-stream velocity (vortex amplitude) (—)
λ	vortex wavelength, m
ν	kinematic viscosity, $(\mathrm{m}^2/\mathrm{s})$
ω	Dimensionless wavenumber, $\alpha\theta$ (—)

boundary layer consistent with the existence of counter-rotating vortex pairs were published by Tani and his co-workers in the early 1960s (eg Tani 1962). Measurements were made on a number of different surfaces in two wind tunnels, and it was concluded that characteristics of the experimental arrangement were fundamental to the preferred vortex wavelength. However, it was observed that, once established, the vortex wavelength remained essentially constant in the streamwise direction. (Vortex development at constant wavelength can be represented by lines of constant $G/\omega^{3/2}$ on the stability chart.) These observations have been confirmed by many subsequent experimental investigations.

Once the existence of the instability had been established, some effort was made to confirm the position of the neutral stability curve. Wortmann (1964), in a basic flow free of Görtler vortices on a slightly concave wall, generated disturbances of various wavelengths in a water channel. Using the Tellurium method, he was able to visualise the downstream development of the vortices and, thereby, determine their growth. Bippes (1972), in a comprehensive investigation of Görtler instability, attempted to determine the right-hand branch of the neutral curve by generating different vortex structures and noting whether they were amplified or damped. Bippes also found that, using upstream screens to generate essentially isotropic turbulence, the vortex wavelength was dependent on the flow velocity and surface curvature so that it was close to the most amplified, as predicted by the linear theory. (Similar results have since been obtained by Mangalam et al. (1985) in a low-turbulence wind tunnel.) Furthermore, in a towing tank in which there was no residual disturbances, Bippes found that the emergence of a vortex structure was delayed, although transition occurred in a relatively short distance downstream of the first appearance of the instability.

These results indicate that the appearance and subsequent development of the Görtler instability are influenced by the upstream flow history. Consequently, the receptivity problem for the Görtler instability is likely to be of great importance. It is of interest to note that Kottke (1986) and Finnis and Brown (1989) have described flows for which no vortices were observed.

Much of the previous experimental work, although in some cases investigating vortex development through transition, has often been referred to in terms of supporting the linear theory and illustrating the linear growth region of Görtler instability. Nonlinear growth of the vortex structure exhibits larger vortex amplitudes leading to points of inflexion in the upwash velocity profiles as well as in the spanwise velocity variation (Wortmann 1969; Aihara and Koyama 1981; Swearingen and Blackwelder 1987). The nonlinear growth is followed by a meandering or sinuous flow, the observation of which is reported by most authors investigating this stage of vortex development (Bippes 1972; Aihara 1979; Sabzvari and Crane 1985; Swearingen and Blackwelder 1987). The sinuous flow results from secondary instabilities initiated at the inflexional points in the spanwise velocity profile. A further characteristic of the breakdown of the vortex structure is the formation of horse-shoe or cross-flow vortices at points of inflexion in the upwash velocity profiles. These were visualised by Bippes and Görtler (1972) and mentioned by Swearingen and Blackwelder as an alternative secondary instability to the meandering motion. It is generally agreed that breakdown of these vortices leads to turbulence. Swearingen and Blackwelder suggest a possible mechanism for the Görtler vortex breakdown as being initiated by a rapidly growing temporal instability originating near the surface. They conclude that Görtler vortices do not themselves breakdown to turbulence but rather set up a flow field that is unstable with respect to secondary instabilities.

More recently, Winoto and Low (1989, 1991) have determined the Görtler number at the start of transition at a number of streamwise positions on two concave surfaces. Görtler numbers based on the Blasius mean flow at the start of transition were found to be between 7.5 and 8.0. (Myose and Blackwelder (1991) in a unique investigation in which "natural" vortex wavelengths between 11 and 29 mm could be produced, found that secondary instabilities, characterised by sinuous motion, were initiated at Görtler numbers, based on the Blasius mean flow, of between 7.1 and 8.1.) Riley et al. (1989) performed a similar investigation on two surfaces and also included the effects of free-stream turbulence intensity, which ranged, locally, between 0.5 and 4.2%. They suggested that a further stability parameter, perhaps based on surface curvature, could account for differences between the results obtained on their two surfaces. Zhang et al. (1995) used intermittency profiles at upwash and downwash positions to determine boundary-layer transition. They found the Görtler number based on the Blasius mean flow to be 6.93 at the start of transition.

Winoto and Crane (1980) found that vortex amplitudes reached 30 to 40% of their reference velocity at Görtler numbers of roughly 9 before vortex growth ceased. Vortex unsteadiness was found to occur at Görtler numbers of between 10 and 15 corresponding to values of $\int \beta \, dx$ obtained from the stability chart of Smith (1955) of between 5 and 6. Before vortex breakdown, the spanwise disturbance amplitudes were found to reach as much as 65% of the streamwise amplitudes.

Based on much of the published data, it would seem that, for a zero pressure gradient and constant surface curvature, departure from the expected mean flow, and the linear theory, occurs for $G \approx 6$. The developing instability produces local variations in boundary-layer thickness of 100% or so for $G \approx 8$. These variations produce inflexional velocity profiles in both the spanwise and normal directions leading to time-varying secondary instabilities rapidly breaking down to turbulence. However, it should be borne in mind that, for many of the investigations, the flow regime is chosen so that the Görtler instability is the dominant mode of instability. In naturally occurring flows, rather than the grid-generated, wind-tunnel flows, this is not necessarily the case, and the route to turbulence may be of a very different nature.

This limited review of the literature illustrates many of the uncertainties in predicting the behavior of a laminar boundary layer on a concave surface. There have been few investigations in which experimental data have been compared in detail with a theoretical stability analysis, particularly in the linear growth regime. Theoretical analyses and experimental measurements have tended to be made in isolation, and as a result, comparisons between the two are generally limited. The motivation for the present work was to provide a detailed comparison between the quasiparallel stability analysis and measured data for a zero pressure-gradient flow.

For more detailed discussions and reviews of Görtler instability, the reader is referred to three recent publications: Hall (1990), Floryan (1991), and Saric (1994). These reviews are complementary in that they each approach the subject from a slightly different viewpoint, and together they reflect the current understanding of the behavior of Görtler vortices.

Experimental arrangement

The wind tunnel used to generate the flow investigated was a low-speed, open-return wind tunnel. The flow was generated by a 27-in centrifugal fan upstream of the working section. The fan was driven by a 11.2 kW DC shunt-wound motor, the speed of which was governed by a digital controller. The controller was capable of maintaining the motor set speed to within $\pm 0.01\%$ of full speed (equivalent to an error in fan speed of ± 0.17 rpm or an error of $\pm 0.076\%$ in free-stream velocity at 5 m/s).

The fan discharged across a 9-mm air gap into a 2.4-m high by 2.4-m wide by 3.6-m accumulator containing two baffles. This was followed by a 1.2-m high by 762-mm wide settling chamber containing honeycomb followed by four wire-cloth screens to control the flow turbulence. The aluminium honeycomb had cells 6-mm diameter and 50-mm long. The cloth screens were constructed using 32 mesh, 0.16 mm wire diameter stainless steel wire cloth having an open area of 64%. The settling chamber was followed an 8.9 : 1 two-dimensional (2-D) contraction to an exit of 135-mm high by 762-mm wide.

Immediately upstream of the working section, the floor boundary layer was removed with a passive boundary-layer bleed at a sharp leading edge. The bleed, which provided a distinct origin for the boundary layer in the working section, added a 100-mm flat plate lead-in to the start of the curved surface.

The curved working section was constructed of clear plastic sheet mounted on medium-density fibreboard formers supported in a steel square-section tube frame. The lower surface of the working section was 2000-mm long by 762-mm wide with a constant radius of curvature of 4 m. Static pressure tappings were placed every 100 mm in the streamwise direction across the center 150 mm of the span. The surface curvature was such that, in this tunnel at the free-stream velocities for which measurements were made, breakdown to turbulence was through the mechanism of Görtler instability.

The upper surface of the working section was made of clear plastic sheet suspended at ten streamwise positions. In the upper surface, were 10 spanwise slots, 250-mm by 13-mm, which enabled a probe to be positioned at different streamwise positions in the working section. Unused slots were filled with balsa wood plugs to ensure continuity of the underside of the upper surface. The roof position could be altered at the suspension points allowing adjustment of the streamwise pressure gradient.

For the results presented here, the roof was adjusted to give a nominally zero pressure gradient or constant velocity. For the streamwise extent of interest (up to a streamwise position of $\approx$1400 mm), the variation in free-stream velocity, based on the static pressure variation, was less than +0.3%, −0.2% up to a nominal free-stream velocity of 10 m/s.

Velocity measurements were made using a constant temperature hot-wire anemometer mounted on a probe support extending through one of the slots in the upper surface of the working section. The probe used was a gold-plated boundary-layer probe with a sensitive length of 1.25 mm (DANTEC model 55P05). The probe was mounted with the sensor approximately 62 mm upstream of the probe support, which was attached to a stepper motor-driven, three-axis traversing mechanism. This allowed the hot-wire sensor to be traversed parallel to the surface across the span of the working section.

Spanwise traverses outside of the boundary layer indicated that the free-stream velocity varied by less than 0.5% of the mean. Traverses perpendicular to the surface showed that the normal velocity gradient could be ignored. For example, at the sixth streamwise position, the normal velocity gradient, based on measurements just outside of the boundary layer, was approximately $0.2U_0$/m (where U_0 is the nominal free-stream velocity). Free-stream turbulence intensity values were less than 0.15% at all of the streamwise positions at which measurements were made.

A Pitot static tube and K-type thermocouple were mounted in the air stream at the exit of the working section in order to monitor free-stream conditions. All pressures were read using a micromanometer having full-scale ranges of 1 and 10 mm water (gauge).

Probe traversing, data acquisition, tunnel operation, and subsequent processing were performed using an IBM-compatible PC. Voltages from the anemometer and micromanometer were read using a 16-bit A/D converter with a voltage range of ±5 V. The thermocouple output was read using a 12-bit A/D converter with programmable gain.

All of the measurements presented here were made as spanwise velocity profiles. The general procedure used when making the measurements was, firstly to position the probe accurately relative to the surface in the absence of the flow using the hot-wire anemometer as a proximity transducer. Secondly, the hot-wire was calibrated in the working section of the wind tunnel before each profile was measured. The tunnel working-section velocity was then set, the free-stream velocity measured, the spanwise profile taken, and finally, the measurement of the free-stream velocity was repeated.

Results and discussion

At each of six streamwise positions, a series of spanwise velocity profiles was made at nominal free-stream velocities of 7.5 m/s and 10 m/s. The profiles of streamwise velocity were measured over the centre 200 mm of the span of the working section, with a resolution of 1 mm.

The free-stream velocities of 7.5 m/s and 10 m/s are similar, and most of the detailed results are presented for 7.5 m/s. When considering streamwise development of the vortices, particularly in terms of growth paths through the stability chart, it is appropriate to consider a single free-stream velocity. However, if development is considered in terms of Görtler number, the results at the two velocities can be combined to give a more detailed picture of the growth and breakdown of the flow structure.

The spanwise profiles were made within the boundary layer at increments in height of 10% of the local Blasius boundary-layer thickness until there was no discernible spanwise variation of streamwise velocity. Before (and after) each profile was measured, the free-stream velocity and ambient temperature and pressure were noted. The local Blasius boundary-layer thickness (99%) was determined from $\delta_L = 4.91x/\mathrm{Re}_x$, and the profile was measured at the required height. The variation of Blasius boundary-layer thickness for a set of spanwise profiles at a single streamwise position and velocity was generally less than ±1%.

Figure 1 shows the streamwise development of the spanwise profiles at a height of $0.4\delta_L$. The increasing spanwise variation with increasing streamwise position is entirely consistent with the Görtler instability. The troughs in the profiles are associated with regions of upwash, where the effect of adjacent vortices is to move low-momentum fluid near the wall up into the boundary layer. The peaks in the profiles are associated with regions of downwash, where fluid higher up in the boundary layer is brought closer to the wall by the action of the vortices. Initially, the variation in the profiles is small and centred about the expected Blasius velocity (shown by the dotted lines in the figure). The variation in the streamwise velocity component increases in size to the streamwise position $x = 1190$ mm, after which the amplitude decreases and the average velocity departs from the Blasius value. As shown later, the precise behavior of the spanwise velocity profiles depends on where within the boundary layer they are measured. In comparing the profiles, it can be seen that many features are common to both free-stream velocities; peaks and troughs can be identified as occurring at roughly the same spanwise positions. (This was also the case for free-stream velocities of 5 m/s and 12.5 m/s.) The detail of profiles is slightly different because the peaks and troughs do not occur at exactly the same spanwise positions. However, they do occur at the same spanwise locations at different streamwise positions for the same free-stream velocity.

Figure 2 shows the streamwise development of the contours of streamwise velocity at a free-stream velocity of 7.5 m/s. The

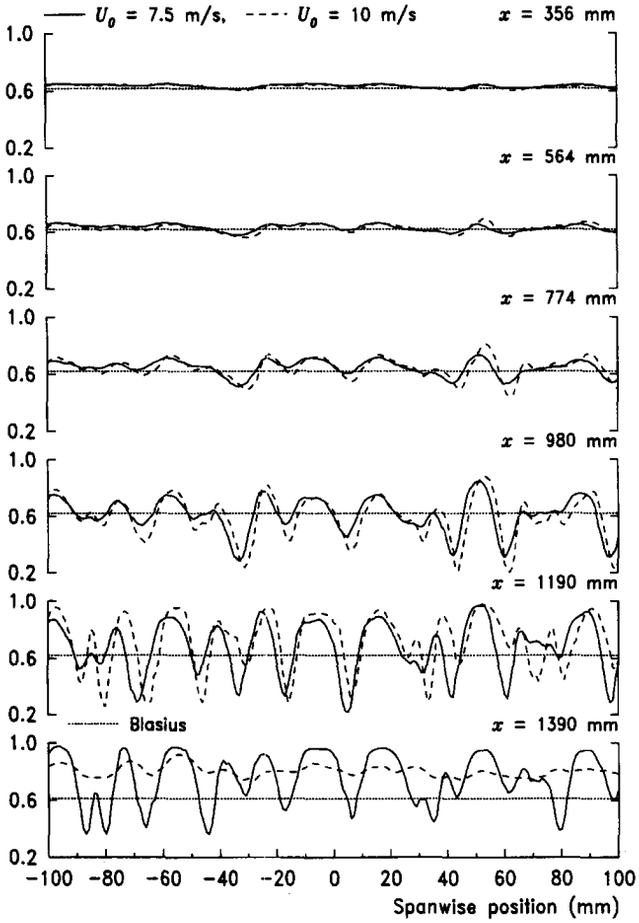

Figure 1 Streamwise development of the spanwise variation of u/U_0 at $y=0.4\delta_L$ for $U_0 \approx 7.5$ m/s and $U_0 \approx 10$ m/s

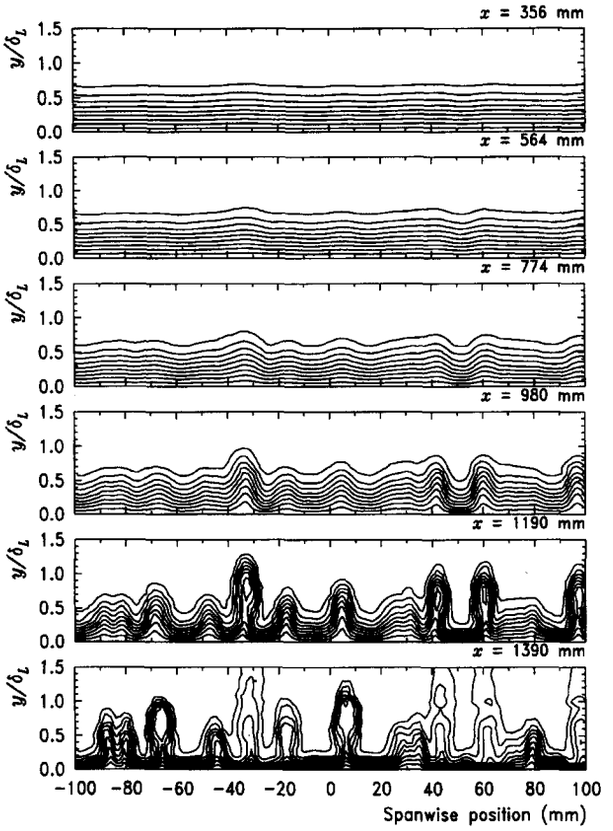

Figure 2 Streamwise development of contours of u/U_0 for $U_0 \approx 7.5$ m/s: contours from 0.1 to 0.9 in steps of 0.1

upwelling of the boundary-layer flow is far more apparent than in the previous figure. The boundary layer develops from a relatively undisturbed flow to a highly distorted boundary layer in which the spanwise variation in boundary-layer thickness is quite remarkable. This is particularly evident in the region about the spanwise position of 50 mm. The figure shows that the breakdown of the flow is initiated at regions of upwash and also that, once the flow starts to breakdown, it does so in a fairly short streamwise distance. Also evident from Figure 2 is that the vortex pairs (there is a vortex either side of each upwelling) are not particularly evenly spaced across the span.

To determine the development of the mean flow and estimate the average vortex growth, boundary-layer profiles were determined using mean and rms velocities obtained from each spanwise profile. Figure 3 shows the streamwise development of the mean boundary-layer flow at the two free-stream velocities. The mean flow remains very close to the Blasius profile up to $x = 980$ mm at 7.5 m/s and up to $x = 774$ m at 10 m/s. After these streamwise positions, the mean boundary-layer profile becomes distorted and thicker than the Blasius profile, until at $x = 1390$ mm at 10 m/s, the mean profile is close to a turbulent seventh power-law profile. Before the average profile thickens dramatically, the trend is for velocities close to the wall to be higher than the Blasius values and velocities further from the wall to be lower than the Blasius values. This is because of the extremes of the variation in streamwise velocity having a lower limit of zero at the wall, tending to raise the average value low in the boundary layer, and an upper limit of the free-stream velocity tending to lower the average value high in the boundary layer. This also indicates why the profiles of Figure 1 at a height of $0.4\delta_L$ are roughly centred about the Blasius value for most of their development. As can be seen from Figure 3, the average velocity at height $0.5\delta_L$ is very close to the Blasius profile for all of the profiles shown.

Figure 4 shows the streamwise development of the profiles of the rms values obtained from the spanwise profiles. These profiles might be expected to represent an average disturbance profile across the span and that the amplitudes might represent in some way an average vortex amplitude. (This is certainly true of the theoretical model, in which the spanwise variation of streamwise velocity at a particular height is assumed to be

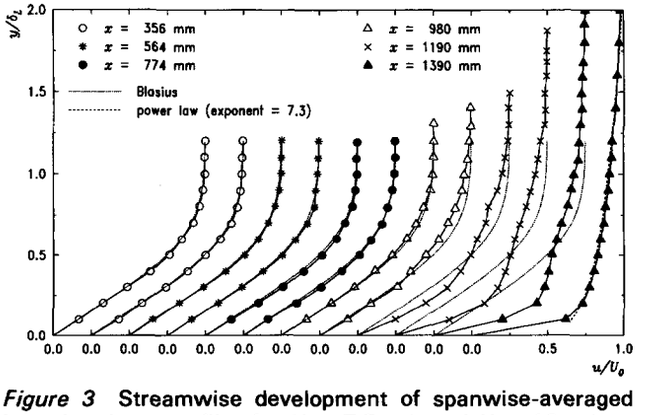

Figure 3 Streamwise development of spanwise-averaged boundary-layer profiles for $U_0 \approx 7.5$ m/s and $U_0 \approx 10$ m/s

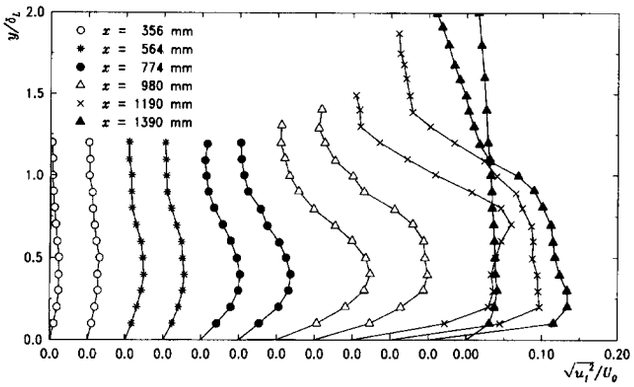

Figure 4 Streamwise development of spanwise-averaged disturbance profiles for $U_0 \approx 7.5$ m/s and $U_0 \approx 10$ m/s

sinusoidal. Hence, the profile of the rms velocities will be the disturbance profile scaled by $1/\sqrt{2}$.) Consequently, the growth of the amplitude of the rms profiles represents the average vortex growth, at least for small amplitudes. The solid symbols in Figure 5 show the variation of amplitude with streamwise position for the two free-stream velocities. As can be seen, the growth of the disturbance amplitude is roughly exponential to $x \approx 1000$ mm for both free-stream velocities, after which the rate of increase reduces until the amplitude decreases as the flow breaks down to turbulence. The exponential growth of the disturbance amplitude extends beyond the streamwise position for which the mean flow can be considered to be Blasius, as indicated by the profiles of Figure 3. The slopes of the straight lines shown in the figure correspond to the constant values of vortex growth rate β assumed in the normal-mode analyses. The values obtained from Figure 5 are 3.71/m at 7.5 m/s and 3.78/m at 10 m/s.

So far, there has been no reference to the theory or, indeed, any of the stability parameters. To place the measured data on a stability chart, it is necessary to determine a Görtler number G and a wave number ω. Because the mean flow under investigation is essentially the Blasius boundary layer, the Görtler number is evaluated from the theoretical mean flow rather than the measured mean flow (for small disturbances these are one and the same).

It will be recalled that for each set of spanwise profiles, the streamwise position is known, as well as the 99% Blasius boundary-layer thickness (determined from the flow conditions

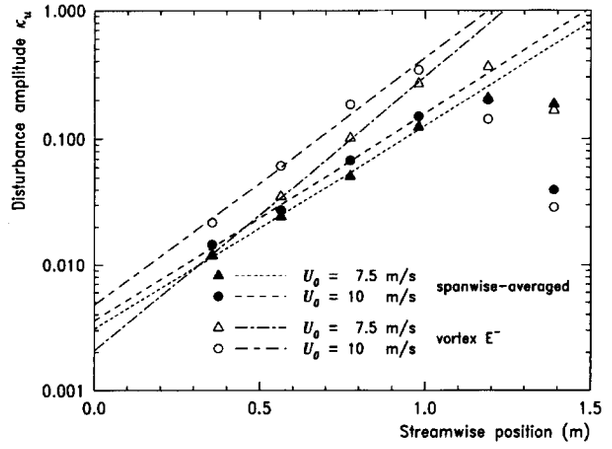

Figure 5 Streamwise variation of disturbance amplitudes for $U_0 \approx 7.5$ m/s and $U_0 \approx 10$ m/s

at the time of measuring the profile). Because the boundary-layer thickness is given by

$$\delta_L = 4.91x/\sqrt{\mathrm{Re}_x} \tag{1}$$

then

$$\sqrt{\mathrm{Re}_x} = 4.91x/\delta_L \tag{2}$$

and as the momentum thickness θ is given by

$$\theta = (\theta/\delta)x/\sqrt{\mathrm{Re}_x} \tag{3}$$

where $(\theta/\delta) \approx 0.664$, then the Görtler number G is given by

$$\mathrm{G} = \mathrm{Re}_\theta(\theta/r)^{1/2} = (\theta/\delta)^{3/2}\left(\sqrt{\mathrm{Re}_x}\, x/r\right)^{1/2} \tag{4}$$

where r is radius of curvature of the surface.

Table 1 shows the Blasius boundary-layer parameters evaluated for both free-stream velocities. It must be stressed that these parameters are based on the anticipated mean flow and can only be expected to have any significance at streamwise positions for which the measured mean flow is close to the anticipated mean flow. Referring back to Figures 5 and 3, it can be seen from the table that the streamwise extent for which the mean flow remained close to the Blasius flow corresponds to Görtler numbers between 6 and 7. Exponential growth continued to streamwise positions corresponding to Görtler numbers of between 7 and 8.5. These agree with previously reported "transitional" Görtler numbers (e.g., Winoto and Low 1989, 1991; Myose and Blackwelder 1991).

For the Blasius mean flow, it can be shown (e.g., from Equation 4) that $\mathrm{G}^{4/3} \propto x$, where the constant of proportionality is given, in a similar manner to the above, by

$$(\theta/\delta)^2(U_0 r/\nu)^{1/3}/r = (\theta/\delta)^2\left(\sqrt{\mathrm{Re}_x}\right)^{2/3}(r/x)^{1/3}/r \tag{5}$$

Figure 6 shows the variation of the spanwise-averaged disturbance amplitudes with $\mathrm{G}^{4/3}$. In the figure, straight lines have been fitted to the first four points at each free-stream velocity. However, these eight datapoints could be considered to lie on a single line. It is not clear whether this is a coincidence or

Table 1 Blasius boundary-layer parameters

x (mm)	$\delta_{L_{av}}$ (mm)	$\mathrm{Re}_x \times 10^{-5}$	θ (mm)	Re_θ	G	ω (global)
	Nominal free-stream velocity, 7.5 m/s					
356	4.17	1.76	0.564	279	3.306	0.204
564	5.26	2.77	0.712	350	4.662	0.260
774	6.17	3.80	0.834	409	5.910	0.304
980	6.80	5.01	0.919	470	7.128	0.337
1190	7.66	5.83	1.035	507	8.155	0.380
1390	8.21	6.92	1.110	552	9.201	0.408
	Nominal free-stream velocity, 10 m/s					
356	3.60	2.36	0.487	323	3.559	0.177
564	4.57	3.68	0.618	403	5.004	0.227
774	5.34	5.06	0.723	472	6.349	0.264
980	5.74	7.02	0.777	556	7.753	0.284
1190	6.69	7.62	0.905	580	8.723	0.334
1390	7.05	9.36	0.954	642	9.923	0.345

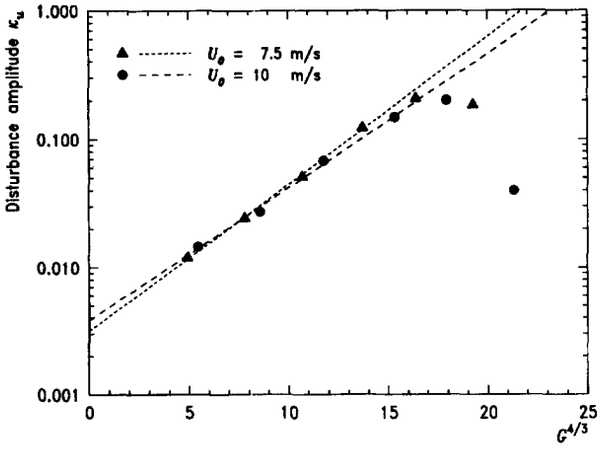

Figure 6 Variation of spanwise-averaged disturbance amplitudes with $G^{4/3}$ for $U_0 \approx 7.5$ m/s and $U_0 \approx 10$ m/s

whether amplitudes at other free-stream velocities would also lie on the same line. Because there is no obvious reason why this should be, two lines have been drawn. The slopes of these lines are related to β through Equation 5. Using average values of $(U_0 r/\nu)^{1/3}/r$, the growth rates obtained from Figure 6 were 3.66/m for both free-stream velocities. These are slightly lower than the values obtained from Figure 5. This is probably attributable to the effect of averaging $(U_0 r/\nu)^{1/3}/r$ over all of the streamwise positions at each free-stream velocity.

To evaluate wave numbers for the experimental data, it is required to determine disturbance wavelengths. Harmonic analyses of the spanwise profiles were made to obtain estimates of average, or global, wavelengths. It was found that, for many spanwise profiles, wave numbers corresponding to a wavelength of roughly 17 mm were dominant in the spectrum for both free-stream velocities. (This was also found to be the case at 5 m/s and 12.5 m/s.) For other spanwise profiles, where the amplitudes were very small; for example, high in the boundary layer and for streamwise positions, up to 564 mm, there were wave number peaks in the spectrum corresponding to 17 mm although the dominant wave numbers tended to be smaller. The wave numbers based on the Blasius mean flow and global wavelengths are also shown in Table 1.

Figure 7 shows the experimental data plotted on the universal stability chart for Blasius mean flow. Because the wavelength essentially remains constant in the streamwise direction, the data lie roughly parallel to lines of slope 3/2 on the stability chart. (It is easily shown that for a constant wavelength, the parameter $G/\omega^{3/2}$ is a constant. The often quoted parameter $\Lambda = U_0\lambda/\nu(\lambda/r)^{1/2}$ is simply $(2\pi)^{3/2}G/\omega^{3/2}$.) The data lie in a region of the stability chart in which much of the previously published data can be found. This region of the stability chart is also a region for which lines of constant growth rate obtained from the normal-mode analysis are also roughly lines of constant wavelength, as shown in Figure 7. In this respect, the normal-mode analysis does reflect the two observed characteristics of the instability.

Given the Görtler number and the wave number, the normal-mode analysis can be used to obtain a value of nondimensional growth rate $\beta\theta\,Re_\theta$ and a disturbance velocity profile. Because the disturbance velocities are the eigenfunction in the normal-mode analysis, only the shape of the profile is available, not the amplitude. Figure 8 shows the streamwise development of the theoretical disturbance profiles compared with the measured profiles for a free-stream velocity of 7.5 m/s. The measured profiles are those of Figure 4, and all of the profiles

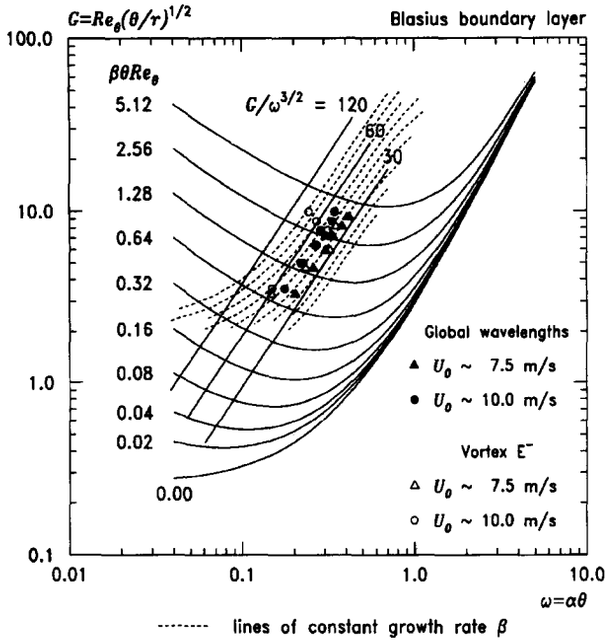

Figure 7 Stability parameters based on Blasius mean flow

have been normalised with their maximum values. (The maximum value of a measured profile was taken to be the maximum value of a cubic polynomial fitted round the peak of the profile.) For both velocities, the theoretical profile at $x = 356$ mm is slightly fuller than the measured profile. There is reasonable agreement between the theoretical and measured profiles for the next two streamwise positions, after which the mean flow departs from the Blasius flow, and the vortex amplitudes are such that the linear analysis cannot be expected to apply. The theoretical profiles for 7.5 m/s and 10 m/s are almost identical at the same streamwise positions; however, the profiles, both theoretical and measured, do vary with streamwise position. The measured profiles at $x = 356$ mm seem to compare better with the theoretical profiles of the next streamwise position, although this may be caused by errors introduced by the small amplitudes at $x = 356$ mm.

Figure 9 shows the values of $\beta\theta\,Re_\theta$ obtained using the normal-mode analysis plotted against $G^{4/3}$. It can be shown that the slope of this curve is $\beta(U_0 r/\nu)^{1/3}/r$, and because $(U_0 r/\nu)^{1/3}/r$ is simply a function of the mean flow and the

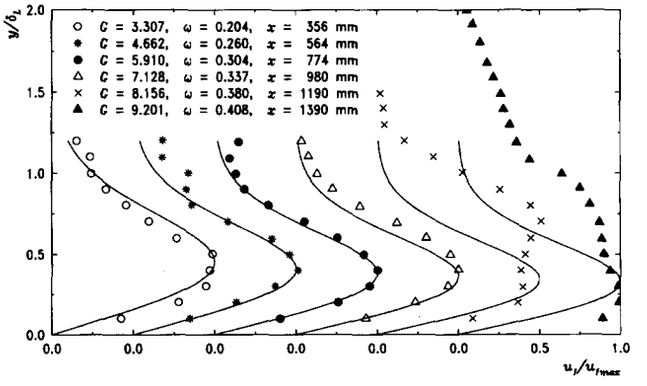

Figure 8 Streamwise development of disturbance-velocity profiles for $U_0 \approx 7.5$ m/s: symbols are spanwise-averaged values, solid lines are theoretical profiles

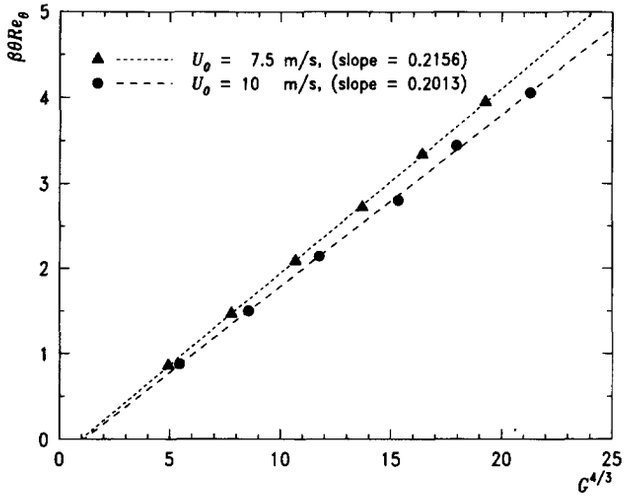

Figure 9 Variation of nondimensional growth factor $\beta\theta\,Re_\theta$ with $G^{4/3}$

surface curvature, the slope is directly proportional to the growth rate β. (The constant of proportionality is obtained is a manner similar to that of Equation 5.) As can be seen from the figure, the data lie in straight lines, again confirming that the normal-mode analysis predicts constant growth rates for the measured flow. However, the values of growth rate obtained from slopes of the lines are 6.77/m at 7.5 m/s and 6.98/m at 10 m/s, which are far larger than the measured values of roughly 3.6/m. The two most likely reasons for this are:

(1) The theoretical model is inadequate. This is known to be the case, as outlined in the Introduction. The normal-mode analysis, although agreeing reasonably well with the experimental results in a qualitative manner, is understood to predict higher growth rates than those predicted using the marching scheme, as well as those likely to be encountered in practice.

(2) The flow is not that modelled by the theory. This would seem to echo the above. However, the linear theory assumes a sinusoidal variation of disturbance velocity across the span, which is not necessarily realized in practice. As shown below, this can affect the average growth rates quite markedly.

Figure 10 shows the spanwise profiles through the boundary layer, relative to the average velocities, at $x = 980$ mm and a free-stream velocity of 7.5 m/s. Also shown are contours of turbulence intensity, which clearly show the positions of the vortex pairs. The figure also shows the relationship between the vortex positions and the locations of the peaks and troughs in the spanwise profiles. Although the streamwise position is just downstream of the small amplitude disturbances, the figure does allow a number of vortex pairs to be identified and located at streamwise positions upstream. The five prominent pairs are denoted A to E in the figure, with the superscripts $^-$ and $^+$ indicating counterclockwise and clockwise rotation (looking downstream), respectively. As can be seen, the vortex pairs are of different strengths and are separated by regions of relatively undisturbed flow, with vortex pairs D and E being the only adjacent pairs in this region of the span. This is reflected in the spanwise profiles, in which the peaks and troughs are of different magnitudes across the span, and adjacent peaks and troughs are not always centred about the mean velocity.

The analysis of the spanwise profiles described above was repeated for only those parts of the profile contained within the vortex pairs denoted A to E. This gave slightly higher growth rates, as shown in Table 2, because of the relatively undisturbed flow being ignored. However, the growth rates were still far less than the theoretical values. The analysis was also repeated for the individual vortex pairs. The growth rates, also shown in Table 2, are higher again than when considering all of the vortices. This is partly because of the variation in mean velocity for each vortex

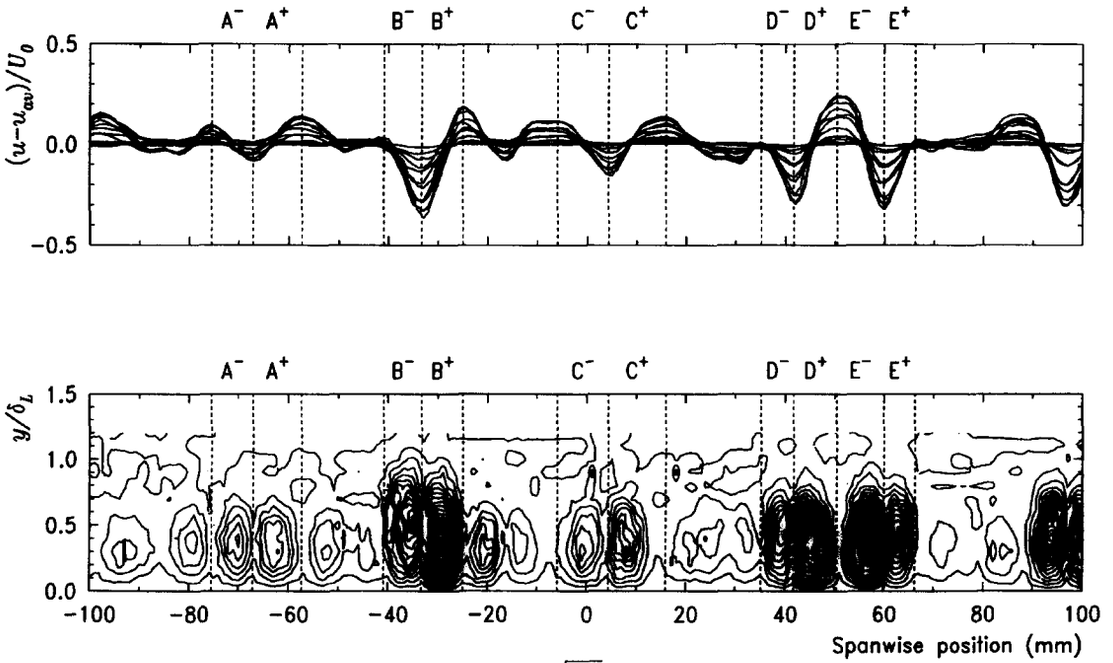

Figure 10 Spanwise variation of $(u - u_{av})/U_0$ and contours of $\sqrt{u'^2}/U_0$ at $x = 980$ mm and $U_0 \approx 7.5$ m/s: contours from 0.6 to 12.0% in steps of 0.6%

Table 2 Values of growth rate obtained from the streamwise development of the disturbance amplitudes

Vortex pair	Vortex	Nominal free-stream velocity 7.5 m/s	10 m/s
	A^-	4.570	5.704
A		4.325	5.233
	A^+	—	5.152
	B^-	4.795	5.019
B		4.367	4.477
	B^+	4.368	4.479
	C^-	4.331	4.309
C		4.418	4.458
	C^+	4.473	4.567
	D^-	—	—
D		4.586	4.732
	D^+	4.594	5.125
	E^-	5.121	5.112
E		5.101	4.587
	E^+	—	6.102
Spanwise averaged		3.713	3.784
Averaged over A, B, C, D & E		3.922	3.961

pair due to the asymmetric pattern of the two peaks and trough, and its effect when evaluating an rms value across a number of pairs. However, the effect of weaker vortices on either side of a vortex pair, or, indeed, no vortices at all, will have the effect of reducing the growth rate of the pair, as compared with the theoretical ideal. Note that when evaluating wave numbers, there is a choice of wavelengths that can be used, either the global wavelengths, as before, or average wavelengths based on the vortex pairs considered.

The theory can be considered to model a counter-rotating vortex pair with an identical vortex pair on either side. As is evident, the pairs should contain an upwash with downwash positions being located between the pairs. Extending the argument to a single vortex (because the only difference in the theoretical vortices is their sense of rotation), a comparison can be made between adjacent upwash and downwash profiles. Because the theoretical spanwise variation in velocity is sinusoidal, the downwash peak and upwash trough should be centred about the mean velocity, and, for the linear theory, the velocity profile midway between upwash and downwash should be identical to the average of the upwash and downwash profiles, which should be equal to the mean flow. Referring to Figure 10, it can be seen that vortices D^+ and E^- come closest to satisfying the above conditions and are perhaps the vortices most likely to be represented by the theory. It is of interest to note that vortex pair E breaks down first (contours of u/U_0 for $U_0 = 10$ m/s at $x = 1390$ mm showed vortex pair E as the only pair breaking down in a similar manner to vortex pairs B, D, and E in Figure 2).

Figure 11 shows the streamwise development for the boundary-layer profiles for vortex E^- at a free-stream velocity of 7.5 m/s. The upwash, downwash, and midposition profiles were obtained from linear interpolation of the spanwise profiles at each height. The spanwise positions of upwash and downwash were estimated using the turning points of the spanwise profiles at heights of $0.2\delta_L$. As can be seen the midposition, and average profiles are close to the Blasius profile up to $x = 774$ mm. At $x = 980$ mm, the average profile has deviated slightly from the Blasius profile, and by the following streamwise position, the average profile is far from Blasius, and the highly distorted upwash profile has the characteristic "S" shape of large amplitude vortices.

In calculating wave numbers for the individual vortex, there are a number of wavelengths that can be used: the wavelength based on E^-, the wavelength based on the pair E^- and E^+, or even the wavelength based on D^+ and E^-. Figure 7 shows the data placed on the stability chart using the wave numbers based on the single vortex E^-. The data are more variable than data based on global wavelengths, indicating that there is some local adjustment of wavelength as the vortex develops. The last two points at a free-stream velocity of 10 m/s are displaced because of the vortex breaking down. In placing the data on the stability chart, using other possible choices of wavelength, the data become fairly scattered, although all of the data, apart from the last point at a free-stream velocity of 10 m/s, lie between the lines of $G/\omega^{3/2} = 30$ and 60. However, if this is repeated for all of the vortices, the variability of the data is increased substantially, and the simplicity of the data based on global wavelengths is lost.

In Figure 12, the measured disturbance profiles for vortex E^- at 7.5 m/s are compared with the theoretical profiles corresponding to the data of Figure 7. The measured profiles are determined from half the difference between the downwash and upwash profiles. Apart from the profile at $x = 356$ mm, there is reasonable agreement between the measured and theoretical profiles to $x = 980$ mm.

The hollow symbols in Figure 5 show the streamwise variation of the disturbance amplitude for vortex E^-. The slopes of the curves, and hence, the growth rates, for the two free-stream velocities are 5.12/m at 7.5 m/s and 5.11/m at 10 m/s. Although still lower than the theoretical growth rates, they are higher than the other growth rates obtained from the data. As can be seen from Table 2, the more locally the vortices were considered, the higher the growth rates obtained. The highest growth rates were obtained from individual vortices that were closest in their immediate environment to the theoretical model. It is probable that, should the vortex pairs be evenly spaced across the span and to be of similar amplitude, the spanwise-averaged growth rates would be higher and would approach those predicted by the linear stability analysis. If this were the case, the theory could be used for engineering purposes, because it would predict the highest vortex growth rates likely to be encountered in a particular flow. Also, in this case, the variability of the individual vortex data on the stability chart could be ignored, and the simplicity of the global data, based on the mean flow and a representative wavelength, could be used.

This also has implications for investigations of heat and mass transfer in the presence of Görtler vortices. To ensure that individual measurements reflect values that could occur in a system of vortices modelled by the theory, an investigation of the flow field should be made to establish the uniformity or otherwise of the vortex structure. It may well be the case that artificially generated systems of vortices would give more reliable results in such investigations.

The disturbance amplitudes indicated by hollow symbols in Figure 5 are the true amplitudes of the vortex rather than the scaled amplitudes indicated by solid symbols. The maximum amplitudes reach about 35% of the free-stream velocity, although the growth rates have started to decrease by this point. The growth rate remains constant up to amplitudes of about 25–30% of the free-stream velocity. The extent of the constant growth rate region in the figure extends to roughly $x = 980$ mm at a free-stream velocity of 7.5 m/s and between $x = 774$ and 980 mm at 10 m/s. The amplitude of the vortices reaches about 10–15% of the free-stream velocity over the streamwise extent for which the mean flow is Blasius, which, as mentioned earlier, corresponds to Görtler numbers of between 6 and 7.

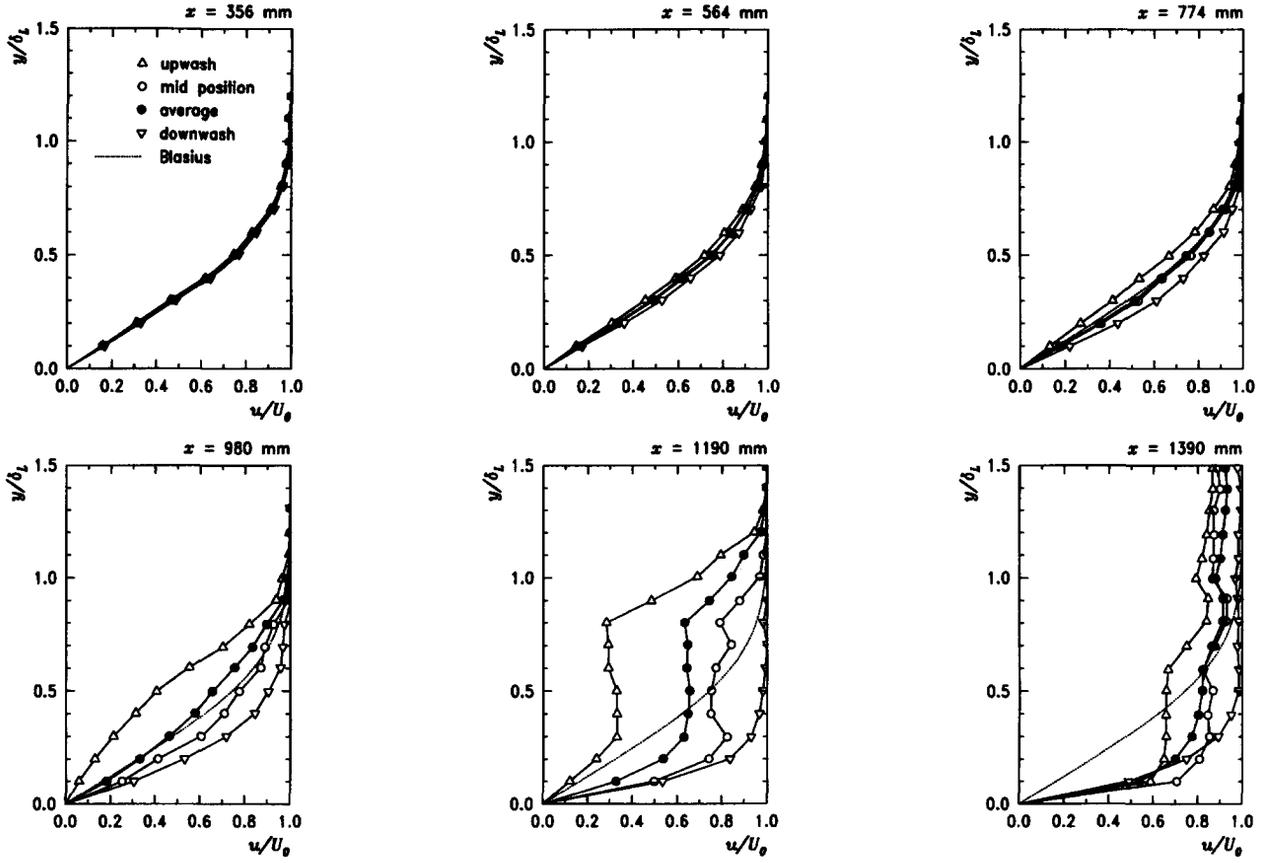

Figure 11 Streamwise development of boundary-layer profiles for cortex E⁻ at $U_0 \approx 7.5$ m/s

Conclusions

Measurements of streamwise velocity within the boundary layer on a constant-curvature concave surface indicated the existence of the Görtler instability. Spanwise velocity profiles showed peaks and troughs that could be associated with regions of downwash and upwash produced by the counter-rotating vortices characteristic of the Görtler instability. The vortices were found to exist in discrete pairs, rather than as a continuous row of counter-rotating vortices, with each pair, often separated by regions of relatively undisturbed flow, centred on a region of upwash.

When using a global description of the vortex wavelength based on harmonic analyses of the spanwise velocity profiles, the streamwise development of the instability was found to be at constant wavelength, although locally, there was some adjustment of wavelength. The wavelength was also found to be independent of free-stream velocity.

The streamwise development of spanwise-averaged velocities was at constant growth rate, which, when suitably nondimensionalised, was similar for both free-stream velocities. Following the linear development of the disturbances, nonlinear growth led to gross distortions of the boundary layer, leading to breakdown of the flow, starting locally at upwash locations.

The spanwise-averaged boundary-layer flow remained close to the expected Blasius mean flow for disturbance amplitudes up to about 15% of the free-stream velocity. This can be considered as the limit of the flow regime for which the linear stability analysis is appropriate. For the present experimental configuration, this corresponded to Görtler numbers of between 6 and 7. The vortices continued to develop at constant growth rate for disturbance amplitudes up to roughly 30% of the free-stream velocity. Further development was at a decreasing growth rate to vortex amplitudes reaching 35% of the free-stram velocity, which corresponded to Görtler numbers of between 7 and 8.5, after which, breakdown to turbulence occurred.

The experimental data lay in the region of the universal stability chart for Blasius flow in which much of the previously published data lie. Disturbance velocity profiles obtained from the stability analysis shows reasonable agreement with the measured profiles at the streamwise positions for which the stability analysis could be expected to apply.

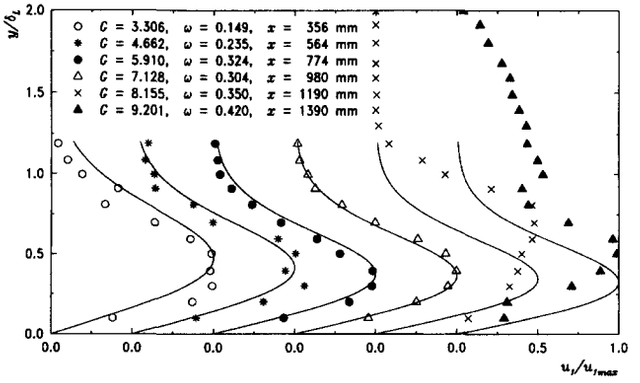

Figure 12 Streamwise development of disturbance-velocity profiles for vortex E⁻ at $U_0 \approx 7.5$ m/s: solid lines are theoretical profiles

Growth rates obtained for the experimental data from the stability chart were much higher than the measured growth rates. This was attributed partly to the normal-mode stability analysis being an ideal solution in the sense of being unattainable in practice. In addition, the growth of the vortex pairs was affected by regions of relatively undisturbed flow adjacent to downwash locations. This is likely to produce lower growth rates than the theoretical analysis, which considers the stability with respect to a single row of counter-rotating vortices.

By considering individual vortices, particularly those that had adjacent vortices, higher measured growth rates were obtained. However, on considering the flow in greater detail, the variability of the resulting data increased, making comparison with the theory more difficult. Although the growth rates of individual vortices were greater than those of average velocities, they were still less than the theoretical growth rates. However, the theory used in making the comparisons was the normal-mode analysis of Görtler instability. It remains to be seen how well the results of a marching scheme would compare with the measured data.

References

Aihara, Y. 1979. Görtler vortices in the nonlinear region. In *Recent Developments in Theoretical and Experimental Fluid Mechanics*, U. Muller, K. G. Roesner, and B. Schmidt (eds), Springer-Verlag, New York, 331–338

Aihara, Y. and Koyama, H. 1981. Secondary instability of Görtler vortices: Formation of periodic three-dimensional coherent structure. *Trans. Japan. Soc. Aero. Space Sci.*, **24**, 78–94

Bippes, H. 1972. Experimentell untersüchung des laminar turbulenten umschlags an einer parallel angeströmten konkaven wand. Heidelberger Akademie der Wissenschaften, Matematischnaturwissenschaftliche klass, Sitzungsberichte, No. 3, 103–180 (Translated as: Experimental study of the laminar-turbulent transition on a concave wall in a parallel flow), NASA TM-75243, 1978

Bippes, H. and Görtler, H. 1972. Dreidimensionale strörungen in der grenzschicht an einer konkaven wand. *Acta Mechanica*, **14**, 251–267

Day, H. P., Herbert, T. and Saric, W. S. 1990. Comparing local and marching analyses of Görtler instability. *AIAA J.*, **28**, 1010–1015

Finnis, M. V. and Brown, A. 1989. Stability of a laminar boundary layer flowing along a concave surface. *J. Turbomech.*, **111**, 376–386

Floryan, J. M. 1991. On the Görtler instability of boundary layers. *Prog. Aerospace Sci.*, **28**, 235–271

Floryan, J. M. and Saric, W. S. 1982. Stability of Görtler vortices in boundary layers. *AIAA J.*, **20**, 316–324

Forest, A. E. 1977. Engineering predictions of transitional boundary layers. AGARD CP-224

Görtler, H. 1940. Uber eine dreidimensionale instabilität laminarer grenzschichten an konkaven wänden. *Ges. d. Wiss. Göttingen, Nachr. a. d. Math.*, **28**(1) (Translated as: On the three-dimensional instability of laminar boundary layers on concave walls), NACA TM 1375, 1954

Gregory, M. A. and Walker, W. S. 1956. The effect on transition of isolated surface excrescences in the boundary layer. ARC TR, Reports and Memoranda No. 2779, part 1

Hall, P. 1982. Taylor–Görtler vortices in fully developed or boundary-layer flows: Linear theory. *J. Fluid Mech.*, **124**, 475–494

Hall, P. 1983. The linear development of Görtler vortices in growing boundary layers. *J. Fluid Mech.*, **130**, 41–58

Hall, P. 1990. Görtler vortices in growing boundary layers: The leading edge receptivity problem, linear growth and the nonlinear breakdown stage. *Mathematika*, **37**, 151–189

Herbert, T. 1976. On the stability of the boundary layer along a curved wall. *Archives Mech.*, **28**, 1039–1055

Kalburgi, V., Mangalam, S. M. and Dagenhart, J. R. 1988a. A comparative study of theoretical methods on görtler instability. AIAA paper 88-0407

Kalburgi, V., Mangalam, S. M. and Dagenhart, J. R. 1988b. Görtler instability on an airfoil: Comparison of marching solution with experimental observations. AGARD CP-438

Kottke, V. 1986. Taylor–Görtler vortices and their effect on heat and mass transfer. *Proc. 8th Int. Heat. Transfer Conference* (San Francisco, CA), 1139–1144

Lee, K. and Liu, J. T. C. 1992. On the growth of mushroom-like structures in nonlinear spatially developing Görtler vortex flow. *Phys. Fluids A*, **4**, 95–103

Liepmann, H. W. 1945. Investigation of boundary-layer transition on concave walls. NACA Wartime Rep. ACR 4J28

Liu, W. and Domaradzki, J. 1990. Direct simulation of transition to turbulence in Görtler flow. AIAA paper 90–0114

Mangalam, S. M., Dagenhart, J. R., Hepner, T. E. and Meyers, J. F. 1985. The Görtler instability on an airfoil. AIAA paper 85–0491

Myose, R. Y. and Blackwelder, R. F. 1991. Controlling the spacing of streamwise vortices on concave walls. *AIAA J.*, **29**, 1901–1905

Riley, S., Johnson, M. W. and Gibbings, J. C. 1989. Boundary-layer transition of strongly concave surfaces. ASME paper 89-GT-321

Sabry, A. S. and Liu, J. T. C. 1988. Nonlinear development of Görtler vortices and the generation of high shear layers in the boundary layer. *Proc. of Symposium to Honor C. C. Lin.* D. J. Benney, F. H. Shu, and C. Yuan (eds.), World Scientific, 175–183

Sabzvari, J. and Crane, R. I. 1985. Effect of Görtler vortices on transitional boundary layers. *Proc. Int. Symp. on Three-dimensional Flow Phenomena in Fluid Machinery*, ASME Winter annual meeting (Miami, FL), 113–119

Saric, W. S. 1994. Görtler vortices. *Ann. Rev. Mech.*, **26**, 379–409

Smith, A. M. O. 1995. On the growth of Taylor–Görtler vortices along highly concave walls. *Quart. App. Math.*, **13**, 233–262

Swearingen, J. D. and Blackwelder, R. F. 1987. The growth and breakdown of streamwise vortices in the presence of a wall. *J. Fluid Mech.*, **182**, 255–290

Winoto, S. H. and Crane, R. I. 1980. Vortex structure in laminar boundary layers on a concave wall. *Int. J. Heat Fluid Flow*, **2**, 221–231

Winoto, S. H. and Low, H. T. 1989. Transition of boundary layer flows in the presence of Görtler vortices. *Exp. Fluids*, **8**, 41–47

Winoto, S. H. and Low, H. T. 1991. Transition of boundary layer flows in the presence of Görtler vortices. *Exp. Fluids*, **10**, 281–284

Wortmann, F. X. 1964. Experimental investigations of vortex occurrence at transition in unstable laminar boundary layers. AF 61(052)-220

Wortmann F. X. 1969. Visualization of transition. *J. Fluid Mech.*, **38**, 473–480

Zhang, D. H., Winoto, S. H. and Chew, Y. T. 1995. Measurement in laminar and transitional boundary-layer flows on concave surfaces. *Int. J. Heat Fluid Flow* **16**, 88–98